**Proceedings of ASME 2010 3rd Joint US-European Fluids Engineering Summer Meeting and 8th International Conference on Nanochannels, Microchannels, and Minichannels**
**FEDSM2010-ICNMM2010**
**August 2-4, 2010, Montreal, Canada**

# FEDSM2010-ICNMM2010-31268

# A PARAMETRIC INVESTIGATION OF OPERATING LIMITS IN HEAT PIPES USING NOVEL METAL FOAMS AS WICKS

**Mahmood R.S. Shirazy and Luc G. Fréchette**
Department of Mechanical Engineering
Université de Sherbrooke
Sherbrooke, Québec, Canada

## ABSTRACT

A parametric investigation has been performed to study the different operating limits of heat pipes employing a novel type of metal foam as wick for chip cooling applications. These foams have a unique spherical pore cluster microstructure with very high surface to volume ratio compared to traditional metal foams and exhibit higher operating limits in preliminary tests of heat pipes, suggesting high cooling rates for microelectronics. In the first part of this parametric study, widely used correlations are applied to calculate the five types of heat transfer limits (capillary, boiling, viscous, entrainment and sonic) as a function of temperature, type of foam, and porosity. Results show that the dominant limit is mostly the capillary limit, but for 50 pore-per-inch (PPI) foam, the boiling limit will be dominant. Also, 50 and 60 PPI foams have higher heat transfer limits than sintered copper powder. In the second part of this study, thermodynamic steady state modeling of a flat heat pipe has been done to study the effect of the different parameters on the dominant limit (capillary). A dimensionless number has been proposed to evaluate the balance between the pressure loss in the vapor and liquid phases as an additional design guideline to improve the capillary limit in flat heat pipes.

## 1. INTRODUCTION

Flat plate heat pipes (FHP) are capillary driven passive devices that are usually used for the thermal management of electronic components. A flat heat pipe is a cavity of small thickness filled with a two-phase working fluid [1]. Heat sources and heat sinks are typically located near the opposite extremities of the heat pipe with the other parts being insulated. Evaporation occurs at the location of the heat sources. The vapour travels along the heat pipe, transporting the extracted thermal energy to the heat sink zones where it condenses. The liquid returns from the condenser to the evaporator through a wick or capillary structure made of micro-grooves, meshes, sintered powder wicks or metal foams. In the field of electronic cooling, working temperatures are in the range of 60 to 120 °C. At this temperature level, the commonly used fluids are acetone, methanol, ethanol or water.

The design and type of capillary structure are main factors that influence the heat transfer capability of a heat pipe [2]. Open cell metal foams are proposed as wicks in flat heat pipes. Metal foams are a good candidate for two phase and single phase chip cooling because they are thermally conductive, light weight, have a high surface area and can provide good thermal contact between the heat pipe wall and the wick. Novel open cell metallic foams can be fabricated with a wide range of porosities, material composition, and microstructures, through a patented process initially developed at the National Research Council, NRC-IMI (Bourcherville, Qc, Canada) and now being manufactured and commercialized by the Canadian company MetaFoam Technologies . These foams have a unique spherical pore cluster microstructure with very high surface to volume ratio compared to traditional metal foams and show good performance for heat transfer applications [3]. In preliminary tests, these foams exhibit higher operating limits in a heat pipe than common wicks, suggesting high cooling rates for microelectronics applications.

Although flat heat pipes are very efficient cooling systems, they are subject to a number of classical heat transfer limitations [4]: continuum flow limit, frozen start-up limit, viscous limit, sonic limit, entrainment limit, capillary limit, condenser limit and boiling limit. These phenomena limit the maximum heat input that may be transported by a heat pipe; heat rates above these limit values result in failure. Frozen-start up limit is not usually encountered in electronics cooling applications and if the condenser is well designed and the heat pipe is free of non-condensable gases, the condenser limit is not typically encountered either.

Modeling of the operation and performance of flat heat pipes has received a lot of attention in two main categories: 1) the numeric or analytic simulation of steady state or transient operation of FHPs, and 2) the transport limits (mainly capillary

 

and boiling) and dry-out lengths. Numerous studies exist on simulations of flow and heat transfer inside FHPs [5,6], transport limits, and dry-out lengths [1, 6-8], but most of these studies are performed assuming a grooved wick structure.

For instance, Lips et al. [1] studied the boiling limit of a transparent flat grooved heat pipe. They showed that the onset of nucleation does not prevent the operation of the FHP and even enhances its performance. Due to experimental challenges, they cannot clearly show that the boiling limit is actually the dominant one (lower than the capillary limit). Dry-out in the evaporator is observed for heat fluxes much higher than the onset of boiling. Hanlon et al. [6] attempted to describe the evaporation process in sintered copper wicks theoretically and by doing experiments. According to them, as the bubbles appear in the wick, the thermal performance of the wick decreases. This result is opposed to [1] and is probably caused by the difference in nucleation mechanisms and bubble growth in grooves and sintered copper. It suggests that the mechanisms involved in failure of a flat heat pipe are not the same for different material wicks and depend on the topology and microstructure of the wicking material.

Only few studies have addressed the application of metal foams as wicks in heat pipes. Phillips [9] studied the permeability, capillary pressures and evaporative performance of different porous materials including high porosity metal foams in order to evaluate their performance as wicks in heat pipes. He concludes that from the capillary pumping point of view, foam wicks are most desirable, felts rank second, and screens are least desirable. But for the onset of nucleate boiling, felts are more convenient than foams. Carbajal et al. [10, 11] and Queheillalt et al. [12] have studied transient response of a large flat heat pipe structure employing nickel foam as a wick, while exposed to a non uniform localized heat flux. Studies to date on metal foams have therefore focused on the wick properties or specific applications, but the relationship between these properties and operating limits remains to be investigated. A survey of the literature does not indicate significant efforts, both at macroscopic and microscopic levels, to study the performance of metal foams in flat heat pipes for electronics cooling applications. Further understanding of phase change alongside capillary driven flow, and also its corresponding relationship to heat pipe limits, are important for efficient flat heat pipes. The current study aims to take an initial step towards this goal.

In order to evaluate the possibility of using the available correlations for calculating the operation limits of a heat pipe with a metal foam wick, and to identify the important design parameters affecting the dominant operating limit, a parametric study has been done in two parts. In the first part, correlations commonly used in the field to calculate the heat pipe limits have been employed to determine different operating limits of a typical circular heat pipe. The circular geometry has been chosen in order to use the existing correlations for ordinary heat pipes. In the second part, thermodynamic steady state modeling of a flat heat pipe has been done to study the effect of the different parameters on the dominant limit, determined in the first part. Here, a rectangular (flat) geometry has been chosen. The main difference between the flat plate and cylindrical geometries is the vapor core cross section. It will be seen that the thickness of the vapor core has considerable impact on the general performance of a FHP. Overall, this device level study will define the research topics that are most critical to further investigate for accurate predictive modeling of FHP with metal foams.

## 2. NOMENCLATURE

| | |
|---|---|
| $A_v$ | Vapour core cross section area ($m^2$) |
| $A_w$ | Wick cross section area ($m^2$) |
| $C$ | Constant depending on Mach number |
| $D$ | Flat heat pipe width (m) |
| $h_v$ | Vapor core height (m) |
| $h_l$ | Wick thickness (m) |
| $K$ | Permeability ($m^2$) |
| $k_{eff}$ | Effective thermal conductivity |
| $L_{eff}$ | Effective length of the heat pipe (m) |
| $L_e$ | Evaporator length (m) |
| $L_c$ | Condenser length (m) |
| $L_{adi}$ | Adiabatic length (m) |
| $M$ | Molecular weight |
| $Ma_v$ | Vapour core mach number |
| $\dot{m}_v$ | Vapor mass flow rate (kg/s.m) |
| $P_{c,m}$ | Capillary pressure (Pa) |
| $P_v$ | Vapour pressure (Pa) |
| $P_l$ | Liquid pressure (Pa) |
| $Q_{tot}$ | Heat power injected in the evaporator (W) |
| $q_d$ | Heat flux ($W/m^2$) |
| $q$ | Heat transfer rate (W) |
| $R_v$ | Vapor constant (J/kg.K) |
| $\bar{R}$ | Universal gas constant (J/ mol.K) |
| $Re_v$ | Reynolds number |
| $r_{h,v}$ | Vapor core radius (m) |
| $r_c$ | Pore capillary radius (m) |
| $r_n$ | Nucleation radius (m) |
| $r_{h,w}$ | Surface pore hydraulic radius (m) |
| $T_\circ$ | Vapor temperature (K) |
| $T_v$ | Vapour temperature (K) |
| $\bar{w}_v$ | Mean velocity of the vapor in the x direction (m/s) |
| $\bar{w}_l$ | Mean velocity of liquid in the x direction (m/s) |
| $\mu_l$ | Liquid viscosity ($N.s/m^2$) |
| $\mu_v$ | Vapour viscosity ($N.s/m^2$) |
| $v_v$ | Vapour kinematic viscosity ($m^2/s$) |
| $v_l$ | Liquid kinematic viscosity ($m^2/s$) |
| $\gamma_v$ | Ratio of the specific heats |
| $\lambda$ | Latent heat of vaporization (J/kg) |
| $\rho_v$ | Vapour density ($kg/m^3$) |
| $\rho_l$ | Liquid density ($kg/m^3$) |
| $\theta$ | Contact angle ($^o$) |
| $\sigma$ | Surface tension (N/m) |

## 3. OPERATING LIMIT CORRELATIONS

### 3.1 Capillary limit

The most commonly studied limitation in flat or miniature heat pipes is the capillary limit [7, 13, 14]. The driving potential for the circulation of the working fluid is the capillary pressure difference. Capillary limit occurs if the maximum capillary

pressure is not enough to overcome the sum of all pressure losses (due to liquid friction, vapour friction, and gravity) inside the heat pipe. This can be expressed as [8]:

$$\frac{2\sigma\cos\theta}{r_c}=\left(\frac{C(f_v\,\mathrm{Re}_v)\mu_v}{2(r_{h,v})^2A_v\rho_v\lambda}\right)L_{eff}q+\left(\frac{\mu_l}{KA_w\lambda\rho_l}\right)L_{eff}q \quad (1)$$

The left-hand term is the maximum capillary pressure produced by the porous structure, where $\sigma$ is the surface tension, $\theta$ is the contact angle (assumed to be zero here) and $r_c$ is the pore capillary radius. The first term at the right side of Eqn 1 expresses the vapour core pressure drop, where $\mu_v$ is the vapour viscosity, $r_{h,v}$ vapour core radius, $A_v$ vapour core cross section area, $\rho_v$ vapour density, $\lambda$ latent heat of vaporization, $q$ is the rate of heat transferred and $L_{eff}$ is the effective length of the heat pipe ($L_{eff}=0.5L_e+L_{adi}+0.5L_c$). The normal hydrostatic pressure is neglected in this equation because of the small inside diameter of the tube. The axial hydrostatic pressure can also be neglected if the heat pipe is assumed to be horizontal. The constant $C$ depends on the Mach number and determines the compressibility of the flow inside the vapour core. The Mach number can be defined as:

$$\mathrm{Ma}_v=\frac{q}{A_v\rho_v\lambda\left(R_vT_v\gamma_v\right)^{1/2}} \quad (2)$$

where $R_v$ is the gas constant, $T_v$ is the vapor temperature and $\gamma_v$ is the ratio of the specific heats (1.33 in this case). The vapor flow regime (laminar or turbulent) can be determined by evaluating the local axial Reynolds number in the vapor. The Reynolds number appears in Eqn 1 as a product with the friction factor: $f_v\,\mathrm{Re}_v$. Reynolds number in the vapor core is defined as:

$$\mathrm{Re}_v=\frac{2(r_{h,v})q}{A_v\mu_v\lambda} \quad (3)$$

The values for these two parameters, C and $f_v\mathrm{Re}_v$, depend on $\mathrm{Re}_v$ and $\mathrm{Ma}_v$, according to:

$$\mathrm{Re}_v<2300 \quad \& \quad \mathrm{Ma}_v<0.2$$
$$f_v\,\mathrm{Re}_v=16 \qquad \mathrm{C}=1.00 \quad (4)$$

$$\mathrm{Re}_v<2300 \quad \& \quad \mathrm{Ma}_v>0.2$$
$$f_v\,\mathrm{Re}_v=16 \qquad \mathrm{C}=\left[1+\left(\frac{\gamma_v-1}{2}\right)\mathrm{Ma}_v^2\right]^{-1/2} \quad (5)$$

$$\mathrm{Re}_v>2300 \quad \& \quad \mathrm{Ma}_v>0.2$$
$$f_v\,\mathrm{Re}_v=0.38\left(\frac{2(r_{h,v})q}{A_v\mu_v\lambda}\right)^{3/4} \qquad \mathrm{C}=1.00 \quad (6)$$

Because the equations used to evaluate both the Reynolds number and the Mach number are functions of the heat transport capacity, it is first necessary to assume the conditions of the vapor flow. Using these assumptions, an iterative procedure must be used to determine the maximum heat capacity. Once this value is known, it can be substituted into the expressions for the vapor Reynolds number and Mach number to determine the accuracy of the original assumption.

The second term at the right side of the Eqn 1 is the liquid pressure drop in the wick. In this term, $\mu_l$ is the liquid viscosity, $K$ is the wick permeability, $A_w$ the wick cross section area, and $\rho_l$ is the liquid density.

### 3.2 Boiling limit

The boiling limit occurs when the applied evaporator heat flux is sufficient to cause nucleate boiling in the evaporator wick. This creates vapour bubbles that partially block the liquid return and can lead to evaporator wick dry-out. They can also violate the curved meniscus interface and hence affect the capillary pumping power [4]. By using the nucleate boiling theory, the boiling limit can be found from the following equation [8]:

$$q_{b,e}=\frac{2\pi L_ek_{eff}T_v}{\lambda\rho_v\ln(r_i/r_v)}\left[\frac{2\sigma}{r_n}-P_{c,m}\right] \quad (7)$$

where $P_{c,m}$ is the capillary pressure in the wicking structure and the nucleation radius $r_n$ is in the range $2.54\times10^{-5}-2.54\times10^{-7}$ m. Due to lack of data for this parameter for metal foam in the open literature, the nucleation radius is chosen to be $2.54\times10^{-6}$ in this study. $k_{eff}$ is the effective thermal conductivity of the porous material.

### 3.3 Sonic limit

The sonic limit is due to the fact that at low vapour densities, the corresponding mass flow rate in the heat pipe may result in very high vapour velocities, and the occurrence of choked flow ($\mathrm{Ma}_v$ reaches 1) in the vapour passage may be possible.The sonic limit can be found from the following equation [8]:

$$q_{s,m}=A_v\rho_\circ\lambda\left[\frac{\gamma_vR_vT_\circ}{2(\gamma_v+1)}\right]^{\frac{1}{2}} \quad (8)$$

$T_\circ$ and $\rho_\circ$ are the temperature and density of the vapor. $R_v$ is the vapor constant ($R_v=\bar{R}/M$).

### 3.4 Entrainment limit

The entrainment limit stems from the case of high shear forces developed as the vapour passes in the counterflow direction over the liquid saturated wick. Here, the liquid may be entrained by the vapour and returned to the condenser. This, results in insufficient liquid flow to the wick structure [15].The entrainment limit can be estimated using [8]:

$$q_{e,m}=A_v\lambda\left[\frac{\sigma\rho_v}{2r_{h,w}}\right]^{1/2} \quad (9)$$

where $r_{h,w}$ is the surface pore hydraulic radius.

### 3.5 Viscous limit

The viscous limit occurs at low operating temperatures, where the saturation vapour pressure difference between the evaporator and the condenser region may be of the same order of magnitude as the pressure drop required for driving the

vapour flow in the heat pipe. This results in an insufficient pressure available to drive the vapour. The viscous limit is sometimes called the vapour pressure limit [15]. Finally the viscous limit can be estimated from the following equation [8]:

$$q_v = d_v^2 \lambda A_v \frac{P_v \rho_v}{4 f_v \mathrm{Re}_v L_e \mu_v} \quad (10)$$

where $f_v \mathrm{Re}_v$ can be found from the Eqns 4 to 6 based on the flow regime.

## 4. TRANSPORT LIMITS FOR A CIRCULAR HEAT PIPE

Dimensions used for this part of the study can be seen in Table 1, representative of industrial applications for microelectronics. These are the dimensions of a typical tube which later is pressed and flattened in order to produce FHP for laptops.

**Table 1. Dimensions of the circular heat pipe**

| Length (m) | Outside diameter (m) | Wall thickness (m) | Wick thickness (m) | Evaporator length (m) | Condenser length (m) |
|---|---|---|---|---|---|
| 0.25 | 0.006 | .0003 | .0007 | 0.02 | 0.03 |

The limiting heat transfers have been calculated for three of Metafoam's metal foams (250, 60 and 50 PPI) as well as for a typical sintered copper powder wick. Table 2 shows the properties of these wicks [16]. The permeability to capillary radius ratios (PCR) is normalized by the PCR of sintered powders. Working fluid is water.

### 4.1 Results for different wick types

In order to determine the dominant transport limit for the 4 types of wick materials, the above limits are calculated and compared in Figs 1 through 4. It can be seen in Figs 1 to 3 that the capillary limit is dominant. The next most limiting phenomena are entrainment at lower temperatures and boiling at higher temperatures. In Fig. 4 however (50 PPI copper foam), the entrainment limit dominates until approximately 60°C, and beyond that, the boiling limit becomes dominant. Due to the high PCR of this foam, its capillary limit is higher than the capillary limit of the other wicks. In all cases, the viscous limit is the most negligible.

As it was mentioned before, while dealing with the numbers obtained for entrainment and boiling limits, one should be careful about the inaccuracies in the correlations used to calculate them.

For the boiling limit, it should be noted that the nucleation radius is not determined for these materials and the value used for this study is chosen to be the average of the upper and lower values of this parameter mentioned in section 3.2. Different values can have significant impact on the numbers obtained as the limits. Also, as it was stated in the literature review, the onset of nucleation cannot be considered as an operational limit. In fact, the correlation which is used in this study for boiling limit is developed without considering the effect of the porous media on the bubble formation and escape. Therefore, the values obtained here should be considered only as a first order estimation and there is a need for a correlation for boiling limit in flat heat pipes using metal foams as a wick.

For the entrainment limit, the wick surface pore hydraulic radius is assumed to be equal to the capillary radius, which is not accurate. For copper mesh wicks this parameter is lower than the capillary radius. With a similar trend for the porous metal foams, then the entrainment limit would be higher than the values obtained here.

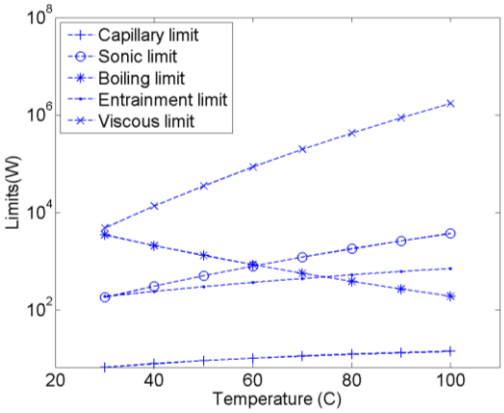


**Figure 1. Different limits for sintered copper powder**

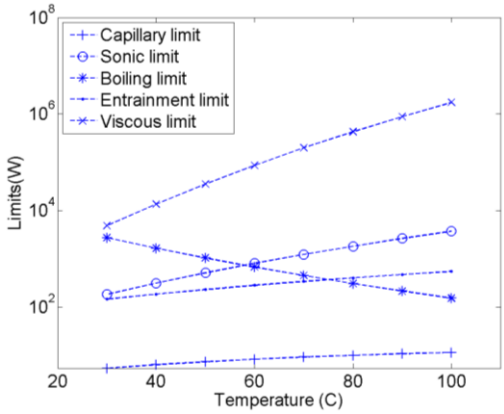


**Figure 2. Different limits for 250 PPI copper foam**

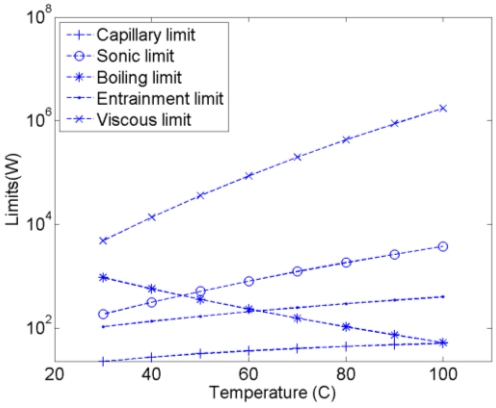


**Figure 3. Different limits for 60 PPI copper foam**

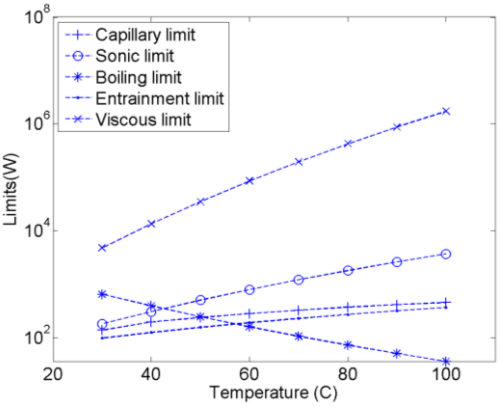


**Figure 4. Different limits for 50 PPI copper foam**

**Table 2. Wick properties** [16]

| Material | Porosity (%) | Thermal conductivity (W/m.K) | Permeability ($m^2$) | Capillary radius( $\mu m$ ) | Normalized PCR ratio |
|---|---|---|---|---|---|
| Sintered copper Powders | 30-50 | 40 | $9.41e^{-12}$ | 27 | 1 |
| Copper foam 250 PPI | 60 | 30 | $1.30e^{-11}$ | 47 | 0.77 |
| Copper foam 60 PPI | 70 | 10 | $1.10e^{-10}$ | 89 | 3.44 |
| Copper foam 50 PPI | 75 | 7 | $1.37e^{-9}$ | 100 | 40.17 |

### 4.2 Results for the Capillary limit

Since the capillary limit is often dominant, the maximum heat transfer capacity of a heat pipe using each type of wick material has been calculated using Eqn 1 for a temperature range of 30 to 100°C. The results are shown in Fig. 5. Basically, it is only the capillary limits calculated in Figs. 1 to 4 which are plotted together to enable comparison. It can be seen that the highest heat transfer capacity occurs with 50 PPI metal foam and this can be attributed to the extremely high PCR of this material. It can be concluded that permeability is the dominant parameter in the effectiveness of theses wick materials. Although the capillary radius increases from 27 to 100 microns (leading to less capillary pumping capacity) the capillary limit increases due to increased permeability (less pressure drop in the liquid section). It implies that for the current geometry and dimensions, the main pressure drop is in the wick (liquid section) and not in the vapor core.

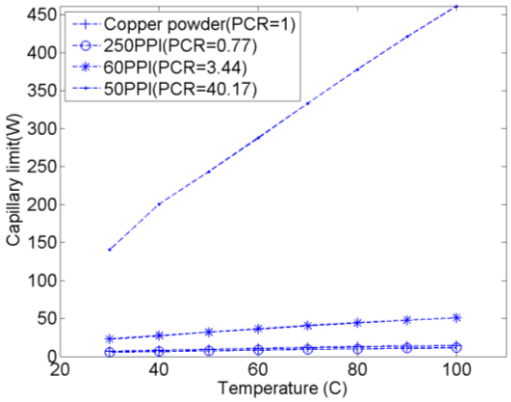


**Figure 5. Capillary limit for different wicking materials**

## 5. PARAMETRIC STUDY OF CAPILLARY LIMIT IN A FLAT HEAT PIPE

As it was observed in the previous part, the dominant limit is mostly capillary limit; therefore it was decided to perform a parametric study to investigate the effect of different parameters on the maximum capillary limit of a flat heat pipe.

This study is different from the previous one in section 4, in the sense that the geometry here is a flat rectangular heat pipe and the vapor core thickness is much smaller than the circular one. The equations and correlations used for this study are the 1-D form of the equations presented in [17], as presented in the following section.

### 5.1 Mathematical model

*5.1.1 Assumptions*

This parametric study is done under the following conditions and assumptions:

- Steady state
- Darcy flow in the wick
- Laminar and incompressible flow in the vapor core
- Working fluid is water
- Axial heat conduction in the wall is ignored

*5.1.2 Capillary pressure*

To estimate the limit, the vapor and the liquid pressure distributions within the device are needed [17]. In this study, evaporation and condensation heat transfer coefficients are not calculated, but instead, all the physics are expressed in terms of the mass and momentum conservation for the two phases, assuming saturation conditions in the phase change zones.

During the normal operation of the heat pipe, the working fluid is constantly flowing from the evaporator to the condenser in vapor state and from the condenser to the evaporator in liquid state. During this path, there are pressure drops in the liquid and vapor phase which should be overcome by the capillary pressure produced at the vapor-liquid interface. The capillary pressure can be expressed as:

$$\Delta P_{cap} = \frac{2\sigma \cos\theta}{r_c} \tag{11}$$

*5.1.3 Vapor phase*

We will derive the vapor pressure from the mass rate balance during evaporation and condensation, as shown in Fig. 6. The conservation law is applied to a control volume and simplifications are made to do the calculations. The control volume is chosen with the height of the vapor core $h_v$ and the length $dx$.

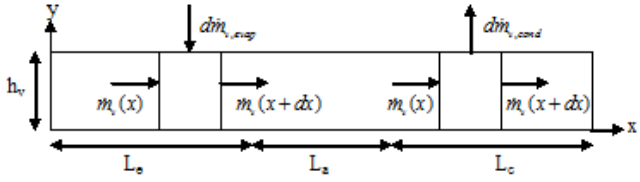


**Figure 6. Vapor core modeling and its corresponding control volumes**

- ***Evaporation***

The pressure distribution inside the vapor core can be calculated from the velocity change due to evaporation and condensation. During the evaporation, as shown in Fig. 6, the absorbed heat can be expressed by the mass flow rate $d\dot{m}_{v,evap}$ entering the vapor control volume D.*dx*.$h_v$. The mass conservation law in this case for the control volume is expressed with Eqn 12:

$$\dot{m}_v(x) + d\dot{m}_{v,evap} = \dot{m}_v(x+dx) \tag{12}$$

The mass flow rate $\dot{m}_v(x)$ could relate to the vapor average velocities in x direction, $\bar{w}_v(x)$, by Eqn 13:

$$\dot{m}_v(x) = \rho_v h_v D \bar{w}_v(x) \tag{13}$$

where, $\rho_v$ is the vapor density, $D$ flat heat pipe width and $h_v$ is the vapor core height. Replacing Eqn 13 in Eqn 12 and simplifying gives the velocity of the vapor phase:

$$\frac{d\bar{w}_v}{dx} = \frac{d\dot{m}_{v,evap}}{\rho_v h_v D dx} \tag{14}$$

The mass flow rate can be expressed by the total heat power, introduced to the evaporator:

$$\frac{d\dot{m}_{v,evap}}{dx} = \frac{\dot{m}_{v,evap}}{L_e D} = \frac{Q_{tot}}{L_e D \lambda} \tag{15}$$

where $Q_{tot}$ is the heat power injected in the evaporator, $L_e$ evaporator length, $D$ flat heat pipe width and $\lambda$ is the heat of vaporization.

- ***Condensation***

Using the same argumentation and procedure, the following equations will be derived for the vapor velocity in the condenser section:

$$\frac{d\bar{w}_v}{dx} = -\frac{d\dot{m}_{v,cond}}{\rho_v h_v D dx} \tag{16}$$

And the heat dissipated in the condenser is expressed by:

$$\frac{d\dot{m}_{v,cond}}{dx} = \frac{\dot{m}_{v,cond}}{L_c D} = \frac{Q_{tot}}{L_c D \lambda} \tag{17}$$

where, $L_c$ is the condenser length. Using the Poiseuille Flow equations to express the laminar flow between the parallel plates, the vapour average velocity is:

$$\bar{w}_v = -\frac{h_v^2}{12\mu_v}\frac{dP_v}{dx} \tag{18}$$

where, $P_v$ is the vapour pressure and $\mu_v$ is the vapour dynamic viscosity. Replacing Eqn 18 in Eqns 17 and 16 will lead to the following relation for vapor pressure distribution:

$$\frac{d^2P_v}{dx^2} = -\frac{12\mu_v}{\rho_v h_v^3 \lambda} q_d \tag{19}$$

where $q_d$ is the heat flux density expressed in Eqn 20 for the three sections of the heat pipe:

$$q_d = \begin{cases} \dfrac{Q_{tot}}{L_e D} & \text{evaporator} \\ 0 & \text{adiabatic zone} \\ -\dfrac{Q_{tot}}{L_c D} & \text{condenser} \end{cases} \tag{20}$$

To have an isolated flow system, where no fluid enters or exits the device, no-flow boundary conditions must be specified:

$$\left.\frac{dP_v}{dx}\right|_{x=0} = \left.\frac{dP_v}{dx}\right|_{x=L} = 0 \tag{21}$$

*5.1.4 Liquid phase*

The liquid flow velocity and pressure distribution in the wick is obtained by the same method as in the case of the vapor velocity. Once again the conservation laws are applied to a liquid control volume during evaporation and condensation:

$$\frac{d\bar{w}_l}{dx} = -\frac{q_d}{\rho_l h_l \lambda} \tag{22}$$

The average axial velocity $\bar{w}_l$ is obtained from the Darcy's law for the liquid flow in porous media:

$$\bar{w}_l = -\frac{K}{\mu_l}\frac{dP_l}{dx} \tag{23}$$

where, K is the wick permeability, $\mu_l$ is the liquid dynamic viscosity, $\rho_l$ the liquid density, $h_l$ the wick thickness, and $P_l$ the liquid pressure. The liquid pressure distribution is:

$$\frac{d^2P_l}{dx^2} = \frac{\mu_l}{K\rho_l h_l \lambda} q_d \tag{24}$$

Again, to have an isolated flow system where no fluid enters or exits the device, no-flow boundary conditions must be specified:

$$\left.\frac{dP_l}{dx}\right|_{x=0} = \left.\frac{dP_l}{dx}\right|_{x=L} = 0 \tag{25}$$

To solve the set of differential equations, a pressure at some point of the system should be assumed to be known. Therefore, the pressure at the end of the condenser section is assumed to be the saturation temperature of the steam at the working temperature.

**5.2 Heat pipe and wick dimensions**

This is a parametric study, in the sense that some of the parameters including the heat pipe and wick properties are changed to see the effect on the capillary limit. Table 3 presents the nominal values that are assumed while changing others. The nominal wick material is the Metafoam 250 PPI foam (Table 2) and the operating temperature is chosen to be 60°C which is the typical operating temperature in practice [3]. The configuration consists of a flat rectangular cross section with wicking layers on both the top and bottom surfaces (total wick material thickness is double the value shown in Table 3).

**Table 3. Dimensions and properties of the nominal FHP**

| Permeability ($m^2$) | Capillary radius ($\mu m$) | FHP length (m) | Evap. length (m) | Cond. Length (m) | Wick thickness (m) | Vapor core thickness (m) | FHP Width (m) |
|---|---|---|---|---|---|---|---|
| 1.30e-11 | 47 | 0.1 | 0.02 | 0.02 | .0007 | 0.0003 | 0.03 |

### 5.3 Results of the parametric study of the capillary limit

*5.3.1 Effect of FHP length*

The length of the FHP has a direct effect on the vapor and liquid pressure drops and hence, affects the capillary limit. The effect of the length is depicted in Fig. 7 and as expected, the maximum heat capacity of the device reduces as the length of the heat pipe is increased. It should be noted that the capillary limit for very short heat pipes reach 80-90 watts, which is probably unrealistic because other limits (boiling for instance) can happen before that. Also, when the length is too short (5 cm in this example); the axial heat conduction along the heat pipe can have a considerable effect on the performance and limits of the heat pipe which is not considered in the current modeling.

*5.3.2 Effect of permeability*

Increasing the permeability can lead to a lower flow resistance and increase the capillary limit. This can be observed in Fig. 8. The typical permeability of sintered copper powder is in the order of $10^{-12}$ and that of metal foams ranges from $10^{-11}$ to $10^{-9}$ (Table 2). It can be seen that for permeabilities up to $10^{-10}$ $m^2$, increasing the permeability of the wick significantly increases the capillary heat transfer limit, but the effect is insignificant above $10^{-10}$ $m^2$. For instance, an increase of two orders of magnitude of the permeability ($10^{-10}$ to $10^{-8}$) leads to only 10% increase of the limiting heat rate.

*5.3.3 Effect of vapor core thickness*

Effect of increasing the vapor core thickness can be seen in Fig. 9. As shown, increasing the vapor core thickness significantly increases the capillary limit. This implies that most of the pressure drop occurs in the vapor phase and not in the wick. Wick thickness is therefore not a limiting parameter in the thermal performance of the FHP configuration studied here. One can suppose that after a certain vapor core thickness, the pressure drops in both phases would have the same order of magnitude and their relative effects would be similar. This can justify the decreasing slope of the graph in the high values of the vapor core thickness. It should be noted that having a high pressure drop in the vapor core leads to a high temperature difference between the condenser and the evaporator, at saturation conditions. This leads to higher overall thermal resistance of the heat pipe.

*5.3.4 Effect of pore radius*

The pore radius has a direct effect on the capillary pumping potential, as a small pore radius will lead to a higher capillary pressure. It can be seen in Fig. 10 that after a pore radius of approximately 100 microns, the effect of this parameter is not that significant.

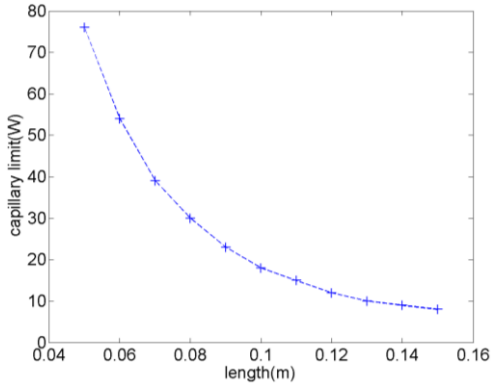


**Figure 7. Effect of FHP length on the capillary limit**

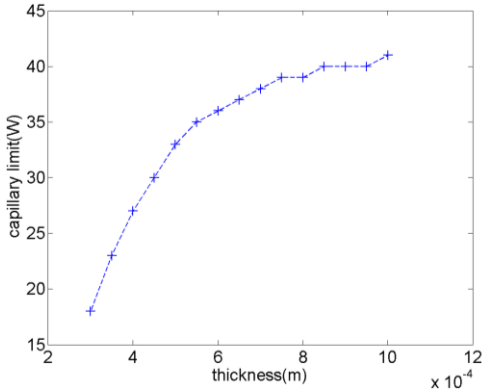


**Figure 9. Effect of vapor core thickness on the capillary limit**

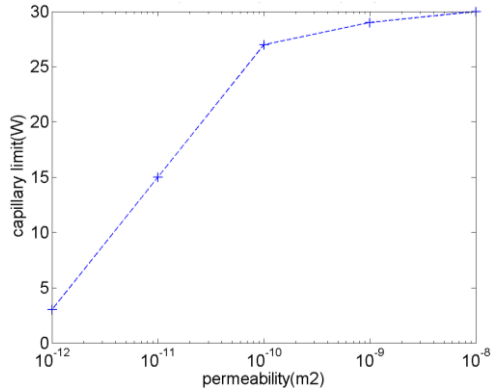


**Figure 8. Effect of permeability on the capillary limit**

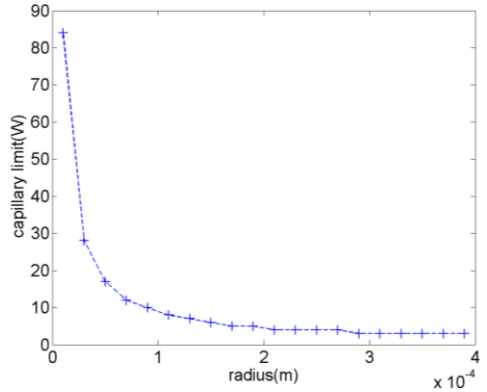


**Figure 10. Effect of pore radius on the capillary limit**

### 5.4 A non-dimensional parameter for capillary limit

By observing Figs 7 to 10, it can be inferred that there should be a parameter that shows the relative importance of the pressure drop in the vapor core to the pressure drop in the wick. It can lead to a design parameter that helps the designer know if he should increase the core or wick thickness and up to what point it is useful. This can be achieved by defining a parameter that includes the ratio of the pressure drop in the vapor core and the pressure drop in the wick. Assuming that $q_c = q_e$, the ratio of Eqn 19 to Eqn 24 will lead to:

$$\frac{\Delta P_v}{\Delta P_l} = 12K \frac{\nu_v}{\nu_l} \frac{h_l}{h_v^3} \tag{25}$$

which combines the effects of the fluid properties (kinematic viscosity ratios), and the geometry at the macroscopic (wick and vapor core dimensions) and microscopic (permeability of the wick) scales. The length and width are the same for both liquid and vapor flow paths and therefore cancel out. A value of 1 for this parameter can be an adequate compromise between both losses. For instance, a value largely over 1 means higher weight of the pressure loss in the vapor core. In this case, the designer can either use a wicking material with a lower permeability, since it's not the limiting parameter (without exceeding the maximum design capillary limit), or change the heat pipe geometry to decrease the vapor pressure drop.

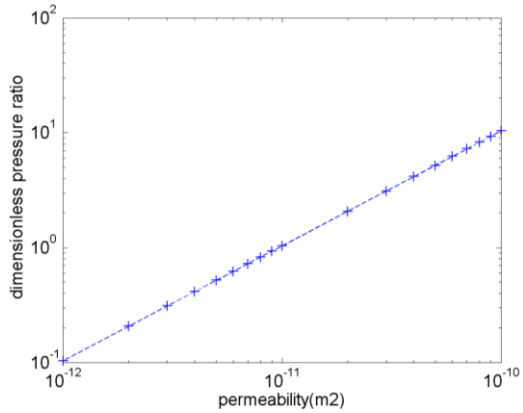


**Figure 11. Effect of permeability on the dimensionless pressure drop ratio**

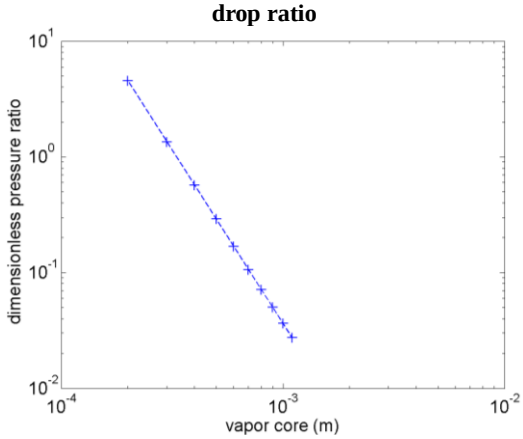


**Figure 12. Effect of vapor core thickness on the dimensionless pressure drop ratio**

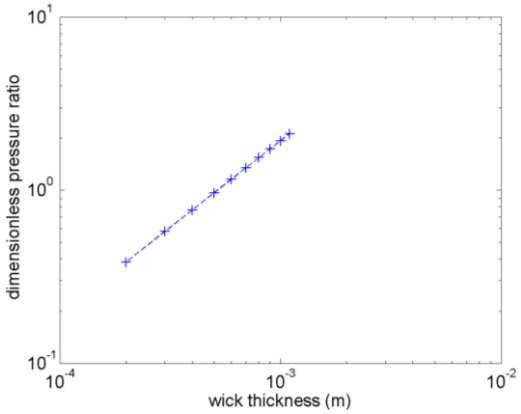


**Figure 13. Effect of wick thickness on the dimensionless pressure drop ratio**

Figures 11 to 13 show the variation of the dimensionless pressure drop ratio (Eqn 25) versus geometrical parameters for the nominal FHP presented in Table 3. Assuming water as the working fluid and an operating temperature of 60°C, this ratio is 1.35 (for the 250 PPI Metal foam) which suggests a balance between liquid and vapor pressure drops.

In Fig. 11, it is obvious that the balanced value for permeability with the current configuration is around $10^{-11}$. Hence, values higher than this leads to a dominant pressure drop in the vapor core. This is consistent with results in Fig. 8. The same conclusions can be made about the results in Figs 12 and 13, showing the relative importance of the vapor core and wick thickness on the pressure drop in the flat heat pipe. By estimating the values of permeability or vapor core thickness that have a noticeable impact on the limit, we can state that there is no more benefit in increasing permeability if the dimensionless pressure ratio is above 10, or in increasing the vapor core thickness if the dimensionless pressure ratio is below 0.1. As a design guideline, a well balanced flat heat pipe should maintain a dimensionless pressure ratio between 0.1 and 10.

### 5.5 Design metrics for FHP

Capillary limit occurs when there is not sufficient driving pressure to overcome the losses in vapor and liquid region. Therefore, a well designed FHP is the result of an effective wicking material, to produce driving pressure, and a minimum flow resistant geometry. In order to evaluate the driving pressure of the wick, PCR can be considered as a good measure. It shows the relative importance of the permeability (wick flow resistance) to capillary radius (driving pressure source). But PCR alone is not enough as criteria to judge a well designed FHP. As it was shown above, when the vapor core is thin, the main pressure loss will happen in the vapor region and this will require a metric to evaluate and choose a pressure balanced geometry. Hence, dimensionless pressure ratio can be used to further judge the pressure losses in the wick and the vapor core. It can help the designer judge his choice of dimensions and make sure that neither the wicking material nor the vapor core overly dominate the pressure losses. Once again, it should be stressed that the current discussion concerns only the capillary limit and boiling limit (the second important limit in electronics cooling application) is not considered here.

## 6. DISCUSSION AND CONCLUSION

Common correlations are used to calculate the dominant limit for circular heat pipes in the conditions usually encountered in electronics cooling applications. Three types of novel metal foams and a typical sintered copper powder have been used as the wicking material in a typical heat pipe configuration. Five types of operating limits have been calculated and the dominant limits were determined, mostly capillary. In the second part of the paper, the capillary limit has been studied in more detail for a flat heat pipe. Finally, a dimensionless parameter has been proposed as a guideline for heat pipe design to evaluate the importance of the pressure losses in vapor and liquid flows.

The conclusions can be summarized as follows:

- The results in the first part (transport limits for a circular heat pipe) confirm the common belief that capillary and boiling limits are the dominant ones in the temperature ranges used in electronics cooling. Entrainment may however become limiting in lower temperature ranges. Also, the theories concerning the boiling limits need to be revised in order to account for the bubble formation in a porous structure.
- The results in the second part of the study (Parametric study of the capillary limit for a FHP) clearly show that the capillary limit is a general function of the wick properties (permeability and pore capillary radius) and geometrical specifications (vapor core thickness, wick thickness, FHP length), assuming a given working fluid. Therefore, designing an effective FHP, i.e. having a high value of heat transfer limit, requires an optimum choice of the geometrical aspects in addition to the transport properties of the wick. A dimensionless number has been proposed to address this issue. Values between 0.1 and 10 represent a balanced pressure loss in wick and vapor core. A good flat heat pipe design should consider both the PCR and this dimensionless pressure loss parameter to keep the balance between the driving force and losses in both liquid and vapor regions.
- Due to the uncertainties that exists in the correlations used in both parts of this study, these first order results are mostly valid to give a preliminary insight into the importance of the different parameters as opposed to providing quantitative predictions. More research is required to establish correlations for capillary and boiling limits, especially for the novel metal foams considered here.

## 7. ACKNOLEDGEMENTS

This research was jointly funded by NSERC Canada and Metafoam Technologies Inc., with the grateful support and guidance of Mr. Dominic Pilon.

## 8. REFRENCES

[1] Lips, S., Lefevre, F., and Bonjour, J., 2009, "Nucleate Boiling in a Flat Grooved Heat Pipe," International Journal of Thermal Sciences, **48**(7) pp. 1273-1278.

[2] Stephan, P., and Brandt, C., 2004, "Advanced Capillary Structures for High Performance Heat Pipes," Heat Transfer Engineering, **25**(3) pp. 78-85.

[3] Pilon, D., 2009, Personal communication.

[4] Faghri, A., 1995, "Heat Pipe Science and Technology," Taylor & Francis Group, United states, pp. 854.

[5] Sonan, R., Harmand, S., Pelle, J., 2008, "Transient Thermal and Hydrodynamic Model of Flat Heat Pipe for the Cooling of Electronics Components," International Journal of Heat and Mass Transfer, **51**(25-26) pp. 6006-6017.

[6] Suman, B., and Kumar, P., 2005, "An Analytical Model for Fluid Flow and Heat Transfer in a Micro-Heat Pipe of Polygonal Shape," International Journal of Heat and Mass Transfer, **48**(21-22) pp. 4498-509.

[7] Williams, R. R., and Harris, D. K., 2006, "A Device and Technique to Measure the Heat Transfer Limit of a Planar Heat Pipe Wick," Experimental Thermal and Fluid Science, **30**(3) pp. 277-284.

[8] Peterson, G.P., 1994, "An Introduction to Heat Pipes: Modeling, Testing, and Applications," Wiley-Interscience, pp. 368.

[9] Phillips, E.C., 1969, "Low-temperature heat pipe research program," Technical Report, CR-66792, NASA.

[10] Peterson, G. P., Carbajal, G., Sobhan, C. B., 2006, "Thermal Response of a Flat Heat Pipe Sandwich Structure to a Localized Heat Flux," International Journal of Heat and Mass Transfer, **49**(21-22) pp. 4070-81.

[11] Carbajal, G., Sobhan, C. B., Bud Peterson, G. P., 2007, "A Quasi-3D Analysis of the Thermal Performance of a Flat Heat Pipe," International Journal of Heat and Mass Transfer, **50**(21-22) pp. 4286-4296.

[12] Queheillalt, D. T., Carbajal, G., Peterson, G. P., 2008, "A Multifunctional Heat Pipe Sandwich Panel Structure," International Journal of Heat and Mass Transfer, **51**(1-2) pp. 312-326.

[13] Chen, S., Hsieh, J., Chou, C., 2007, "Experimental Investigation and Visualization on Capillary and Boiling Limits of Micro-Grooves made by Different Processes," Sensors and Actuators, A: Physical, **139**(1-2) pp. 78-87.

[14] Lefevre, F., and Lallemand, M., 2006, "Coupled Thermal and Hydrodynamic Models of Flat Micro Heat Pipes for the Cooling of Multiple Electronic Components," International Journal of Heat and Mass Transfer, **49**(7-8) pp. 1375-83.

[15] Jalilvand, A., 2008, "Performance Characteristics of Roll Heat Pipe with the Application in the Fusing Roller of Photocopy Machine," Doctoral thesis, Waseda University, Japan.

[16] Metafoam Technologies Inc., 2009, "Copper Foam Properties," **2009**(07/12).

[17] Kamenova, L., Avenas, Y., Tzanova, S., 2006, "2D numerical modeling of the thermal and hydraulic performances of a very thin sintered powder copper flat heat pipe," 37th IEEE Power Electronics Specialists Conference 2006, PESC'06, United States, pp. 1712077.